Section 1
PROGRESS IN LASER FUSION

1.A Numerical Investigation of the Self-Focusing of Broad-Bandwidth Laser Light with Applied Angular Dispersion

The development and application of beam-smoothing techniques[1-6] have produced considerable improvement in laser-irradiation uniformity for inertial-confinement fusion (ICF) laser systems. Some of these techniques act passively [e.g., random phase plates (RPP)[1] or distributed phase plates (DPP)[2]], while others, such as induced spatial incoherence (ISI)[3] or smoothing by spectral dispersion (SSD),[5] are dynamic, calling for the application of broad-bandwidth (BBW) laser light to temporally smooth intensity modulations on target. In this article, we examine the effects of the BBW light used in SSD on the self-focusing of the beam during propagation through nonlinear optical components in the laser system.

The bandwidth used in SSD is in the form of spectrally dispersed, phase-modulated light. Phase modulation is used to minimize the formation of high-intensity spikes that can damage optical materials within the laser system. The spectral angular dispersion serves a dual purpose: it introduces a time-dependent phase variation across the transverse direction of the beam, which leads to intensity smoothing in the far field, and it improves the efficiency of the frequency tripling of the BBW laser light. Both the phase modulation and the angular dispersion enter into the modeling of self-focusing.

Analytic work[7] has shown that spectrally dispersed, phase-modulated beams develop amplitude modulation as they propagate, but this modulation disappears when the beam is brought to an image plane of the diffraction grating. (These calculations have been validated by experiment.[8]) Such modulation is of

particular concern when the beam is injected into a nonlinear medium, such as a lens or a piece of amplifier glass (rod, disk, etc.), where the threat of self-focusing is always present. There are two features of this amplitude modulation that affect the amount of self-focusing that can occur. First, because the angular dispersion imposed by SSD causes the spectral components to sweep across the beam in time, the average intensity will smooth out over a characteristic modulation time. Second, even though the instantaneous amplitude modulation disappears at appropriate image planes within the laser system, any optical components between these image planes must cope with the instantaneous amplitude modulation on the beam. Laser systems that incorporate SSD to improve beam uniformity would benefit from a thorough understanding of this form of amplitude modulation during propagation in a nonlinear medium.

We have developed a multifrequency, multidimensional computer code to examine the effect of SSD on self-focusing for a beam propagating through a laser system. Results from this computer code indicate that, for a given set of SSD parameters and a nonlinear material, there exists a minimum propagation distance for the amplitude modulation created by SSD to begin self-focusing. For distances greater than this minimum, SSD will further enhance the instantaneous self-focusing when the beam is diverging during image relaying, and it will reduce the self-focusing when the beam is converging. In either case, however, because the spatial positions of the intensity spikes are changing in time, the time-averaged intensity is very smooth when averaged over one modulation period.

Simulation results also indicate that SSD smooths the time-averaged intensity of intrinsic amplitude perturbations produced by optical defects in the laser. This is accomplished by the phase gradients across the beam deflecting the perturbation, as the optical rays propagate in the direction perpendicular to the wavefront. Since the phase variation is time dependent and oscillatory, the perturbation is shifted back and forth across the beam within a period of the modulation frequency. When compared with a monochromatic beam, the time-averaged intensity of the perturbation for SSD is therefore reduced due to its energy being spread out over a larger area.

In this article, we first discuss the numerical approximation used to characterize and model SSD propagation. We then validate the model by (a) reproducing the Bespalov-Talanov (B-T) gain curves for self-focusing in a nonlinear medium, (b) examining a simple test of angular propagation using the Talbot effect, and (c) reproducing the analytic results for SSD propagation in air. Finally, we study BBW propagation and self-focusing in a nonlinear medium.

Numerical Method

The derivation of the SSD technique has been given in detail by Skupsky;[5] here we highlight the derivation to illustrate the angular dispersion terms. The laser electric field in a nondispersive material can be written in the form

$$E(\mathbf{r},t) = \Psi(\mathbf{r},t)\, e^{i\phi(\mathbf{r},t)} + \text{c.c.} \;,$$

where the main contribution to the bandwidth for phase-modulated light is

contained in the time-varying phase term $\phi(\mathbf{r},t)$, while $\Psi(\mathbf{r},t)$ represents a more slowly varying pulse-shape term. For the purposes of this calculation, we consider the pulse to be infinitely long and neglect the temporal dependence of Ψ. For sinusoidal phase modulation of the beam, produced by an electro-optic (E-O) crystal, the electric field becomes

$$E(\mathbf{r},t) = \Psi(\mathbf{r})\, e^{i\omega t + i\delta \sin(\omega_m t) - i\mathbf{k}\cdot\mathbf{r}} + \text{c.c.} \ ,$$

where δ and ω_m are the modulation amplitude and angular frequency of the modulation and ω and $\mathbf{k}$ are the fundamental angular frequency and wave number of the laser. Spectral dispersion is imposed upon the beam by means of a diffraction grating. Using the relation

$$e^{i\delta \sin(\omega_m t)} = \sum_{j=-\infty}^{\infty} J_j(\delta) e^{i\omega_m t} \ ,$$

the dispersed electric field becomes

$$E(\mathbf{r},t) = \sum_{j=-\infty}^{\infty} \Psi_j(\mathbf{r}) e^{i(\omega + j\omega_m)t - ik_j z \cos\theta_j} + \text{c.c.} \ ,$$

where $\Psi_j(\mathbf{r}) = \Psi(\mathbf{r}) J_j(\delta) e^{-ik_j x \sin\theta_j}$, with spectral dispersion on the x direction.

The wave number is defined as

$$k_j = \frac{n_o}{c}(\omega + j\omega_m) \ ,$$

where n_0 is the index of refraction, and the angles at which the individual plane waves propagate are determined by the grating dispersion $\Delta\theta/\Delta\lambda$

$$\theta_j = -j\lambda \frac{\Delta\theta}{\Delta\lambda} \frac{\omega_m}{\omega} \ .$$

To examine self-focusing, we calculate the propagation of this beam through a nonlinear medium using the paraxial approximation to the wave equation. The nonlinearity of the refractive index is represented by writing the index as

$$n = n_o + n_2 \langle E^2 \rangle \ ,$$

where the angle bracket indicates time averaging, and the coefficient n_2 is the index of nonlinearity of the medium. The paraxial equation[10] for a monochromatic plane wave then takes the form

$$2i\bar{k}\frac{\partial\Psi}{\partial z} + \nabla_\perp^2\Psi + 2\bar{k}^2\left(\frac{n_2}{n_o}\right)|E|^2\psi = 0 \ ,$$

where $\bar{k} = k_z = |\mathbf{k}|\cos\theta$. Modeling the spectrally dispersed SSD beam requires solving separate equations for each spectral component. However, because of the interfrequency dependency of the four-wave-mixing (4WM) term $\left(\Gamma \equiv |E|^2 E\right)$ it will be necessary to solve this set of equations simultaneously. For 2N spectral components, we have

$$2i\bar{k}_{-N}\frac{\partial\Psi_{-N}}{\partial z}+\nabla_{\perp}^2\Psi_{-N}+2\bar{k}_{-N}^2\left(\frac{n_2}{n_0}\right)\Gamma_{-N}=0$$

$$\vdots$$

$$2i\bar{k}_j\frac{\partial\Psi_j}{\partial z}+\nabla_{\perp}^2\Psi_j+2\bar{k}_j^2\left(\frac{n_2}{n_0}\right)\Gamma_j=0$$

$$\vdots$$

$$\vdots$$

$$2i\bar{k}_N\frac{\partial\Psi_N}{\partial z}+\nabla_{\perp}^2\Psi_N+2\bar{k}_N^2\left(\frac{n_2}{n_0}\right)\Gamma_N=0.$$

where $\Gamma_j=\left(|E|^2 E\right)_j$ represents the 4WM contribution to an individual spectral component.

Four-wave mixing refers to the nonlinear process involving three electromagnetic waves interacting to produce a fourth output wave. It is a third-order process and, as such, is governed by the third-order nonlinear susceptibility.[11] Two of the input waves form a virtual grating, which scatters the third incident wave into the output. The 4WM processes are divided into three groups: self-, cross-, and mixed-phase modulation. These classifications denote the makeup of the three incident waves. Self-phase modulation, or self-focusing, is one of the more noteworthy 4WM processes. Cross-phase modulation involves a wave reflecting back into itself off a virtual neutral grating produced by another wave and its complex conjugate. In mixed-phase modulation the output wave is almost always the product of three waves with completely different frequencies. To illustrate, we consider the 4WM terms for an electric field consisting of three waves traveling in the same direction $E = E_1 + E_2 + E_3$, with

$$E_1 = a_0\exp\left(i\omega_0 t\right)$$

$$E_2 = a_{-1}\exp\left[i\left(\omega_0 - n\omega_m\right)t\right]$$

$$E_3 = a_1\exp\left[i\left(\omega_0 + n\omega_m\right)t\right],$$

where the $i\mathbf{k}\cdot\mathbf{r}$ contribution to the phase has been suppressed. From our general paraxial equation above, we define $\Gamma=|E|^2 E$, where now

$$\Gamma=\left(E_1 + E_2 + E_3\right)\left(E_1 + E_2 + E_3\right)^*\left(E_1 + E_2 + E_3\right).$$

Rewriting, in terms of the exponentials above, we obtain

$$\Gamma = e^{i\omega_0 t}\left(a_0 + a_{-1}e^{-i\omega_m t} + a_1 e^{i\omega_m t}\right)\left(a_0 + a_{-1}e^{i\omega_m t} + a_1 e^{-i\omega_m t}\right)$$

$$\times\left(a_0 + a_{-1}e^{-i\omega_m t} + a_1 e^{i\omega_m t}\right).$$

We now expand this relationship and collect terms for individual frequency components. The contributions to the various frequencies are shown in Table 56.I. It can be seen that the 4WM term for a given frequency is dependent on the other frequencies present due to the cross- and mixed-phase modulation terms, in addition to its own self-phase modulation. Also, the three initial waves serve

Table 56.I: Contributions to different harmonics generated by four-wave mixing for the example of three plane waves. Each term is multiplied by an additional factor of $e^{i\omega_o t}$.

	Self	Cross	Mixed
$e^{-i3\omega_m t}$:			$a_{-1}^2 a_1$
$e^{-i2\omega_m t}$:			$a_{-1}^2 a_0 + 2a_{-1}a_0 a_1$
$e^{-i\omega_m t}$:	a_{-1}^3	$2\left(a_0^2 + a_1^2\right)a_{-1}$	$a_0^2 a_1$
1 :	a_0^3	$2\left(a_{-1}^2 + a_1^2\right)a_0$	$2a_{-1}a_0 a_1$
$e^{i\omega_m t}$:	a_1^3	$2\left(a_{-1}^2 + a_0^2\right)a_1$	$a_0^2 a_{-1}$
$e^{i2\omega_m t}$:			$a_1^2 a_0 + 2a_{-1}a_0 a_1$
$e^{i3\omega_m t}$:			$a_1^2 a_{-1}$

as sources for higher harmonics. This requires that the simulations include a number of higher harmonics whose amplitudes were initially zero.

The simulation code *MCOLORS* is an adaptation of the *MALAPROP*[12] computer code written at Lawrence Livermore National Laboratory. Since *MALAPROP* was written to examine the propagation of a single frequency, a numerical framework was constructed that allows *MCOLORS* to simultaneously propagate all of the frequencies included in an SSD beam. The code propagates each of the individual waves for a spatial step in the z direction and then calculates the coupling terms as described above. A maximum spatial stepsize is determined from the input grid dimensions and the linear and nonlinear refractive indices of the material. The simulation uses finite-difference methods to approximate the paraxial equations and an alternating direction implicit (ADI) numerical scheme to solve the resulting systems of equations. All harmonics were calculated for $|j| \leq 2\delta$, where δ is the modulation amplitude of the E-O crystal. At the grating, the individual wave amplitudes are negligible for harmonics with $|j| \geq \delta$. However, higher harmonics are generated by the 4WM terms during propagation; this is adequately modeled by keeping terms between $\pm 2\delta$.

Verification of Method

Before attempting to model the propagation of a multifrequency laser beam in a nonlinear medium, it was necessary to validate the simulation by reproducing analytic results dealing with self-focusing, angular propagation and SSD propagation in air. Each of these plays a significant role in the propagation of an SSD beam in a nonlinear medium.

1. Monochromatic Self-Focusing in a Nonlinear Medium

The instability of intense laser light propagating within a nonlinear medium has been well established.[13-15] This effect is often responsible for optical damage to laser-system components and, as such, is a limiting factor in the design of high-power laser systems. Linearized instability theory predicts that small amplitude modulations superimposed on a uniform-intensity background will

grow somewhat exponentially with a gain coefficient g given by[13]

$$g = K\sqrt{\frac{n_2}{n_o}\left\langle E^2 \right\rangle - \frac{K^2}{4k^2}} \ ,$$

where K is the wave number of the amplitude modulation, n_2 is the nonlinear refractive index, n_o is the normal index of refraction, $\left\langle E^2 \right\rangle$ is the time-averaged value of the electric field, and k is the wave number of the laser. (As noted by Bliss,[16] the growth is not strictly exponential,[17] but such a description does contain all the qualitative features of a complete treatment.) We can rewrite this equation in terms of the background intensity I as

$$g = K\sqrt{\gamma I - \frac{K^2}{4k^2}} \ ,$$

where I is measured in GW/cm^2 and γ is a nonlinear coefficient defined as

$$\gamma = \frac{4\pi}{c}\frac{n_2}{n_o} \times 10^{16}\frac{cm^2}{GW} \ .$$

Using this formula for the gain coefficient, it is possible to construct a series of curves, as shown in Fig. 56.1, describing the gain coefficient as a function of the nonlinear coefficient γ for the medium. (Here we have chosen the wave number of the modulation to be 120 cm^{-1} and the laser wavelength as 1053.5 nm.) The individual curves represent three different background intensities (2, 3, and 4 GW/cm^2). A series of numerical runs were compiled for each intensity over the range of the nonlinear coefficient. The numerical results appear
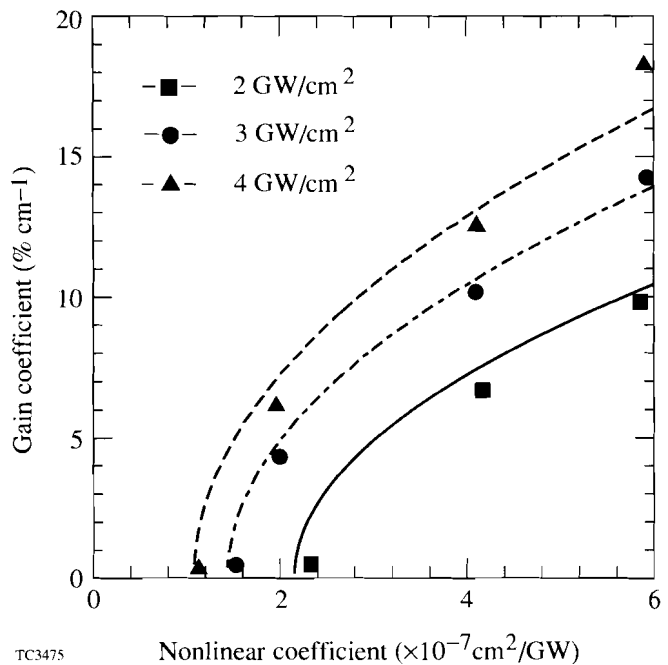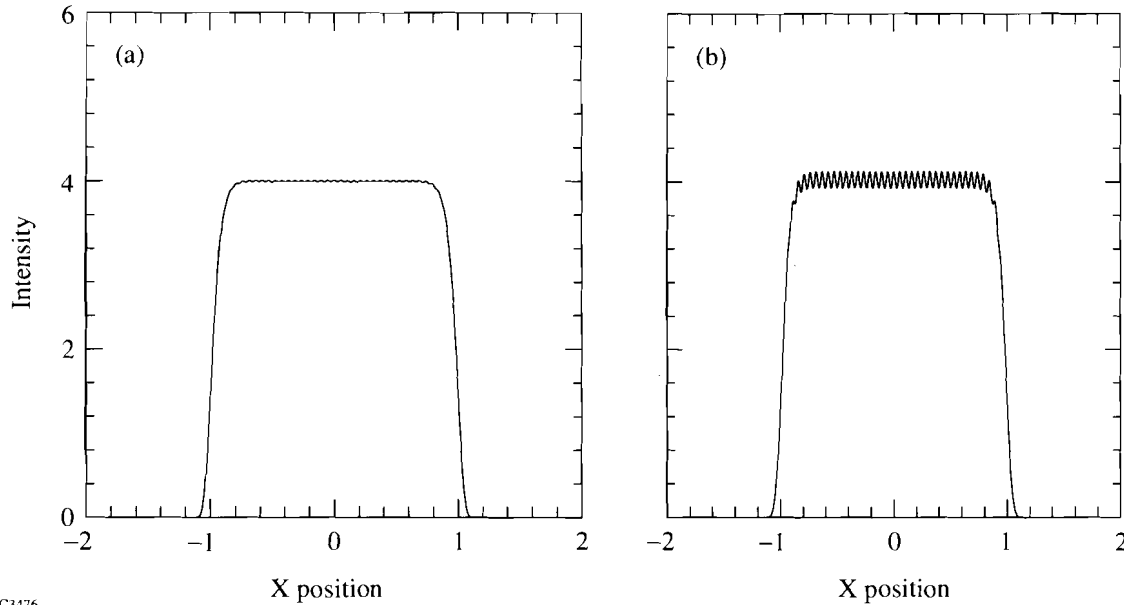

Fig. 56.1
Bespalov-Talanov (B-T) gain coefficient as a function of a nonlinear coefficient γ of the medium. Separate curves are drawn for background intensities of 2, 3, and 4 GW/cm^2. Numerical simulation results for each case are overlaid.

TC3475

in Fig. 56.1 as the various symbols overlaid upon the analytic curves. It can be seen that the simulation is in good agreement with the theory. An example of the 4 GW/cm^2 series is illustrated in Fig. 56.2. The input spatial profile, shown in Fig. 56.2(a), was propagated 25 cm in a nonlinear medium $\left(\gamma = 4.0 \times 10^{-7} \text{cm}^2/\text{GW} \sim 10^{-13} \text{esu}\right)$ and resulted in the growth of the sinusoidal perturbation to that shown in Fig. 56.2(b).

TC3476

Fig. 56.2

Example of the exponential growth of a small sinusoidal intensity modulation on a 4 GW/cm^2 background. (a) Initial spatial profile; (b) spatial profile after propagating 25 cm in a nonlinear material $\left(\gamma = 4.0 \times 10^{-7} \text{cm}^2/\text{GW}\right)$.

2. Angular Propagation

One of the key elements of the SSD method is the imposition of angular dispersion onto the beam. To test that angular propagation was being modeled correctly, we considered solving a simple example of the Talbot effect.[18] Such a test involves the propagation of a field composed of three monochromatic waves traveling in different directions (Fig. 56.3). The Talbot effect maintains that an initial interference pattern in the intensity will repeat itself at distinct positions with uniform spacing along the propagation path. We can determine the location of these positions analytically. The total field is just the summation of the individual plane waves, which we write as

$$E = a_1 e^{-i\mathbf{k}_1 \cdot \mathbf{r}} + a_2 e^{-i\mathbf{k}_2 \cdot \mathbf{r}} + a_3 e^{-i\mathbf{k}_3 \cdot \mathbf{r}},$$

where

$$\mathbf{k}_1 \cdot \mathbf{r} = kz \cos\theta + kx \sin\theta$$
$$\mathbf{k}_2 \cdot \mathbf{r} = kz$$
$$\mathbf{k}_3 \cdot \mathbf{r} = kz \cos\theta - kx \sin\theta .$$

Setting $a_1 = a_3 = 1/4$ and $a_2 = 1/2$, we obtain

$$E = \frac{1}{2}\left[e^{-ikz\cos\theta} \cos(kx\sin\theta) + e^{-ikz} \right].$$

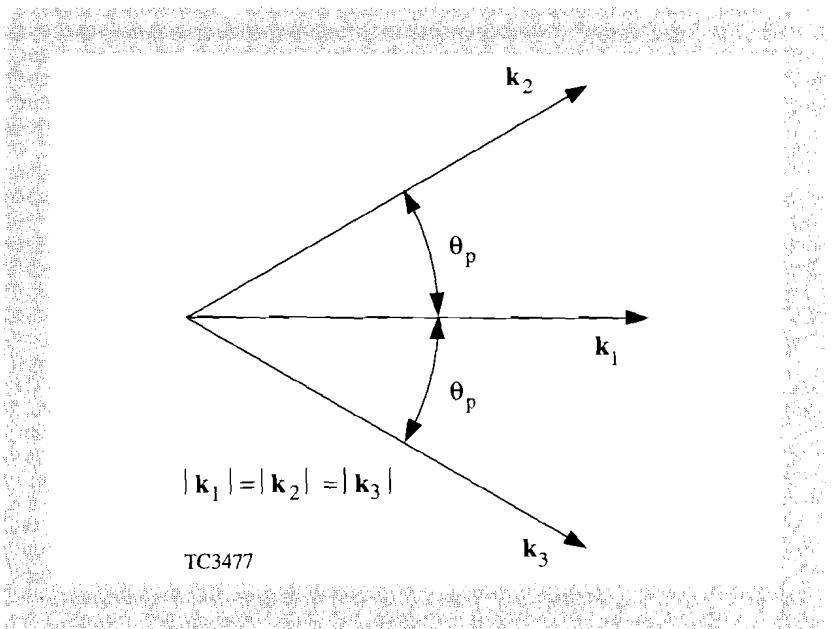Fig. 56.3
Wave-vector alignment for a three-wave angular propagation test. All three-wave numbers are equal, but k_2 and k_3 are traveling at angles $\pm\theta_p$ from k_1 as shown.

Initially ($z = 0$), and at various positions along the propagation path, the two exponential factors will have the same value. This occurs for the condition $kz\cos\theta + 2\pi n = kz$, yielding

$$z = \frac{n\lambda}{(1 - \cos\theta)} \qquad n = 0, 1, 2 \ldots\ldots .$$

At these positions the intensity is given by

$$I = |E|^2 = \cos^4\left(\frac{k\,x}{2}\sin\theta\right) .$$

The intensity pattern for the values $\lambda = 1053.5$ nm and $\theta = 5.0 \times 10^{-4}$ rad is shown in Fig. 56.4(a). We now consider the propagation distance at which the two phase terms above become $90°$ out-of-phase

$$\left[kz\cos\theta + \left(\frac{2n-1}{2}\right)\pi = kz\right] .$$

This leads to

$$z \approx \left(\frac{2n-1}{4}\right)\frac{\lambda}{(1-\cos\theta)} \qquad n = 0, 1, 2 \ldots\ldots ,$$

with the intensity at these positions given by

$$I = \frac{1}{4}\left[\cos^2\left(k\,x\sin\theta\right) + 1\right] .$$

Therefore, if we propagate to the position given by this expression for $n = 1$, we should see a modulated intensity with a maximum intensity of $1/2$, a minimum intensity of $1/4$, and a spatial wavelength $1/2$ the value from the previous example. We calculate the necessary propagation distance to be

(a)   (b)

X position   X position
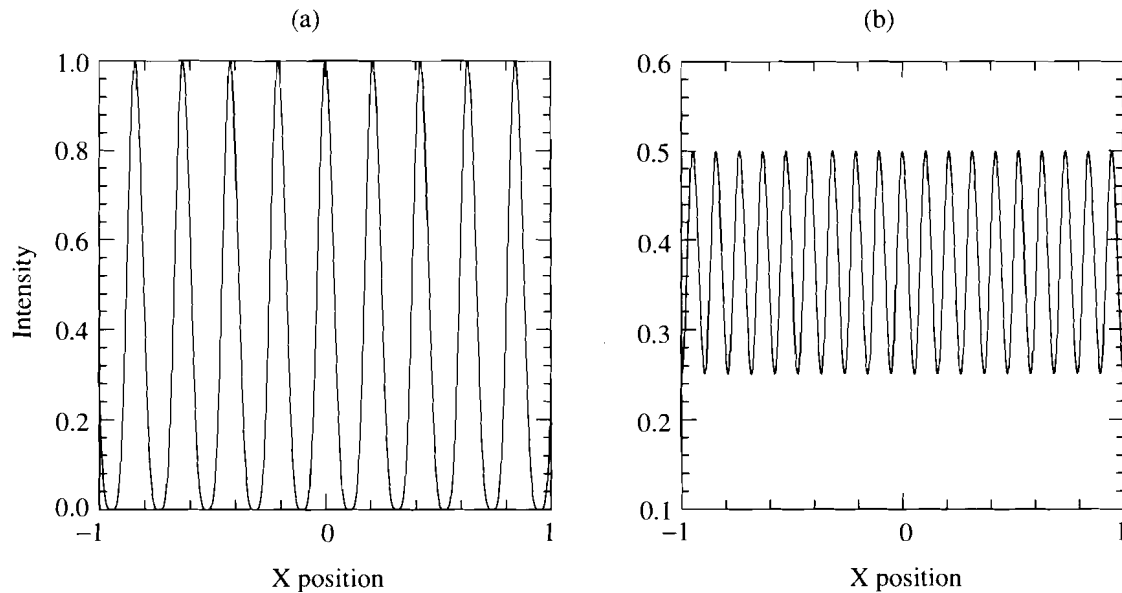
TC3478

Fig. 56.4
Spatial intensity profiles for a three-wave angular propagation test. (a) Initial (z = 0) interference pattern. All three wavelengths are equal to 1053.5 nm, and the propagation angles are $\pm 5.0 \times 10^{-4}$ rad; (b) numerically calculated intensity profile at a propagation distance of z = 210.7 cm. The features of this profile agree well with the analytic predictions.

z = 210.7 cm. The result of an *MCOLORS* run, using these parameters, is shown in Fig. 56.4(b). From this graph it can be seen that the simulation is in good agreement with the analytic result.

3.   SSD Propagation in Air

The last test we examine is modeling the propagation of an SSD beam in air. This problem has been solved previously in an analytic model.[7] This work, verified in experiments,[8] showed that the spectral angular dispersion causes SSD beams to develop amplitude modulation during propagation. As the wavefronts propagate, they become spatially modulated in the transverse direction. This modulation, because of the time-dependent phase, sweeps spatially across the beam in time on successive wavefronts. Picking out a specific point in the propagation path, the analytic model examines the intensity moving past that point as a function of time. Typical results of the analytic model are shown in Fig. 56.5(a). The unperturbed beam started at z = 0 and was propagated 5 m with an E-O modulator frequency of 10 GHz, a modulation amplitude of 4, and a dispersion coefficient due to a diffraction grating of 200 mm/Å. The same parameters were used in an *MCOLORS* simulation to produce the set of amplitude functions (Ψ_j) at the propagation distance of 5 m. The phase terms of the individual spectral components

$$\left[e^{i(\omega_m t - \hat{k}_m z)} \right]$$

of the total electric field were then evaluated in time at a single transverse position of the beam. Comparison of this result [Fig. 56.5(b)] with the analytical result indicates that there is good agreement between the two in predicting the amplitude and period of the intensity modulation.
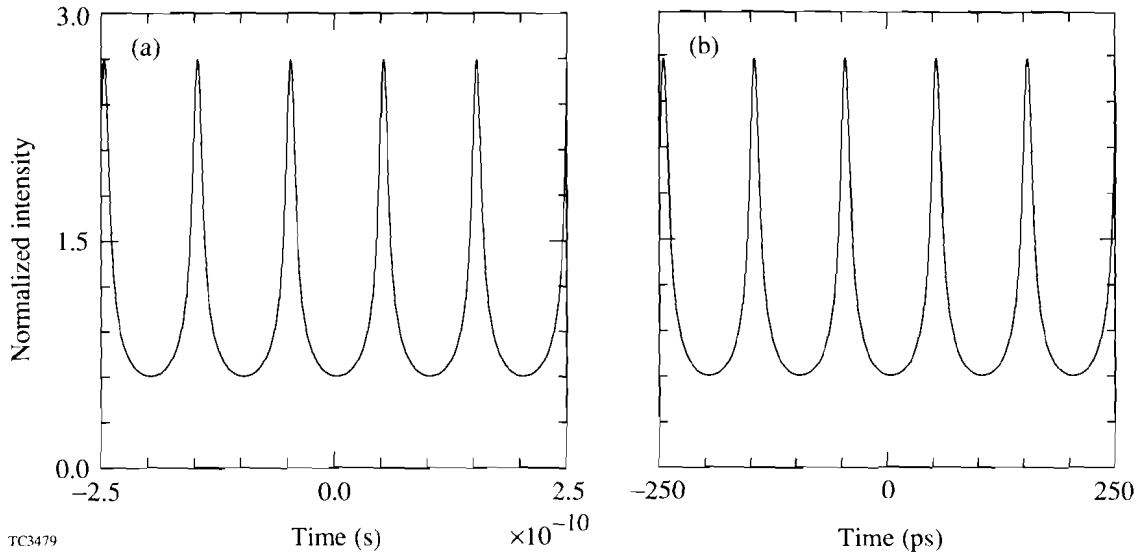
Fig. 56.5
Comparison of analytical calculations and numerical results detailing the accumulated amplitude modulation due to SSD propagation over 5 m. This case involved a modulation frequency of 10 GHz, a modulation amplitude of 4, and a grating dispersion coefficient of 200 μm/Å. (a) Results of the analytic model; (b) results of the numerical simulation.

Propagation of Angularly Dispersed, BBW Light in a Nonlinear Medium

Using the methods described above, we can now examine the propagation and self-focusing characteristics of an SSD beam in a nonlinear medium. We examine two separate scenarios involving phase- and amplitude-modulated beams injected into a nonlinear medium. The first scenario deals with an SSD beam that has developed amplitude modulation solely as a result of propagation. The second scenario involves the study of an SSD beam with an imposed frequency-independent amplitude perturbation on the beam, presumably the result of laser system imperfections.

1. Self-Focusing of Modulation due to Propagation

The self-focusing behavior of an SSD beam as it propagates in a nonlinear material is more easily characterized when the amplitude modulation is allowed to grow to a point where the self-focusing becomes prevalent. There is a critical path length for a given set of SSD and nonlinear material parameters at which self-focusing will begin to occur. As shown in Fig. 56.1, self-focusing occurs when the modulated spikes reach a minimum intensity for a given nonlinear coefficient. Below this value, diffraction will dominate, and the energy in the spike will spread out. A numerical analysis was performed to determine the propagation length required to modulate an SSD beam to such a point that, when injected into a nonlinear medium, self-focusing would begin to occur at a rate of 0.5% cm^{-1}. Using this criterion, we have produced three curves (shown in Fig. 56.6) that illustrate the dependence of the critical path length as a function of the modulation frequency for several cases of bandwidth (3 Å, 9 Å, and 18 Å). (For this set of curves we have chosen the nonlinear coefficient to be $\gamma = 2.9 \times 10^{-7}$ cm^2/GW and the dispersion coefficient to be 200 μm/Å.) From the graph, it can be seen that as one moves to more extreme conditions for SSD (i.e., more bandwidth and higher modulation frequencies), the critical path length gets shorter and shorter. This is due to the shrinking of the transverse

spatial wavelength of the phase modulation in these cases. Since the optical ray propagation is in the direction perpendicular to the wave front, as the gradients in the wave front become steeper, energy within the beam will be pushed into spikes more quickly, and the beam will experience amplitude modulation over a shorter propagation distance.
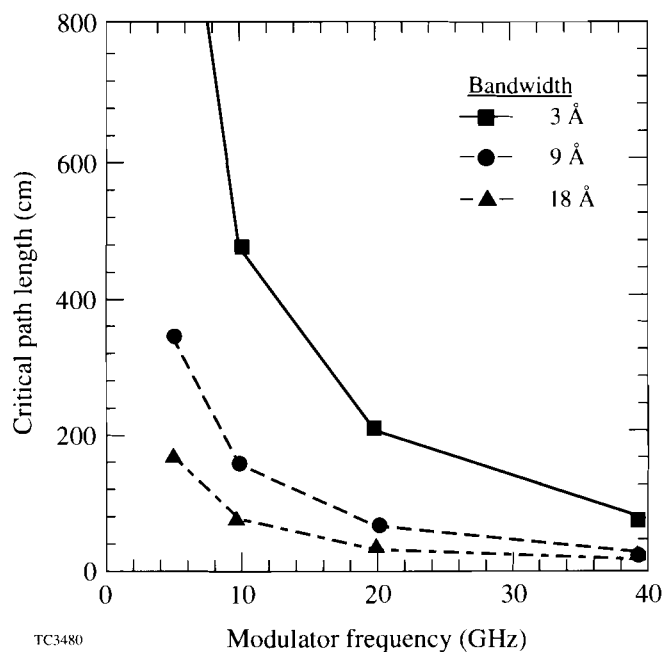
Fig. 56.6
Critical propagation path length for self-focusing (B-T gain coefficient of 0.5% cm^{-1}) as a function of modulator frequency for three separate values of bandwidth (3 Å, 9 Å, and 18 Å).

Using this information, we now propagate a beam a distance greater than its critical path length to observe the effects of SSD on self-focusing. In addition, it should be remembered that since a laser beam is image-relayed as it propagates through a laser system, it is possible that the SSD beam will sample nonlinear material while it is propagating away from (diverging) or toward (converging) an image plane. To examine the difference this has on self-focusing, an unperturbed beam was imposed with 3-Å bandwidth, an E-O modulation frequency of 10 GHz, and a grating dispersion of 200 μm/Å. The initial relative phase distribution is given in Fig. 56.7(a). The beam was then propagated a distance of 550 cm, which resulted in the spatially modulated profile shown in Fig. 56.7(b). Using this profile, we examined the differences in self-focusing over a distance of 50 cm between a diverging SSD beam, a monochromatic beam, and a converging SSD beam. The results of these runs are shown in Fig. 56.8. The monochromatic beam results [Fig. 56.8(b)] serve as a reference for the nominal amount of self-focusing possible. In the case of the diverging SSD beam [Fig. 56.8(a)] it can be seen that the spatial redistribution of the beam energy into spikes due to SSD enhances the overall self-focusing. On the other hand, the converging SSD beam [Fig. 56.8(c)] removes energy out of the spikes and, as such, reduces the amount of self-focusing that takes place. The maximum intensity of the spikes in Fig. 56.8(c) is noticeably lower than the monochromatic reference case in Fig. 56.8(b).
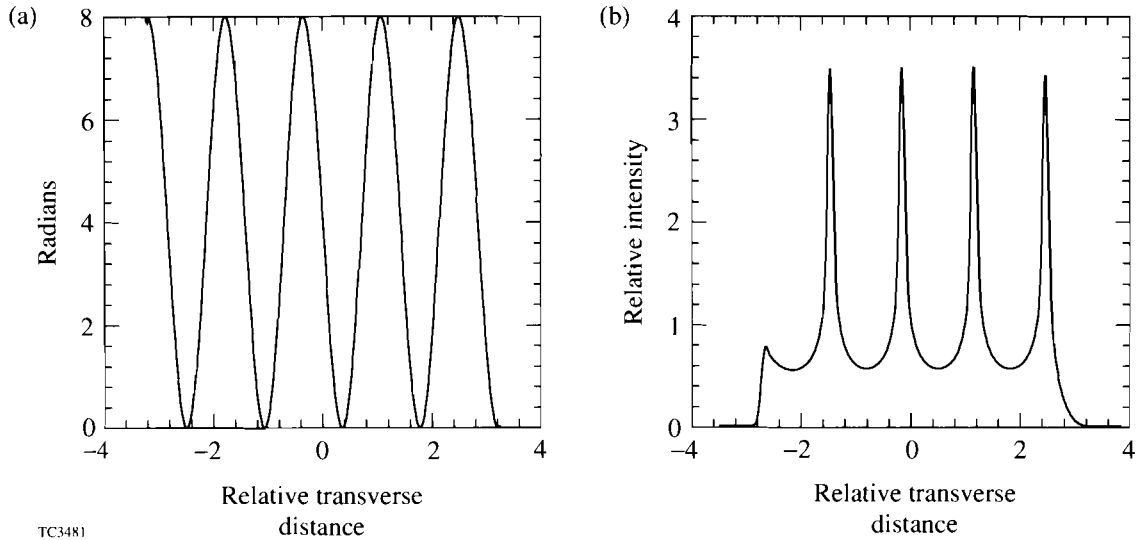
Fig. 56.7

Spatial intensity profile used in examining the effects of SSD on self-focusing in a nonlinear medium. (a) Initial spatial profile of the relative phase distribution across the beam; (b) modulated intensity profile after propagating 550 cm.
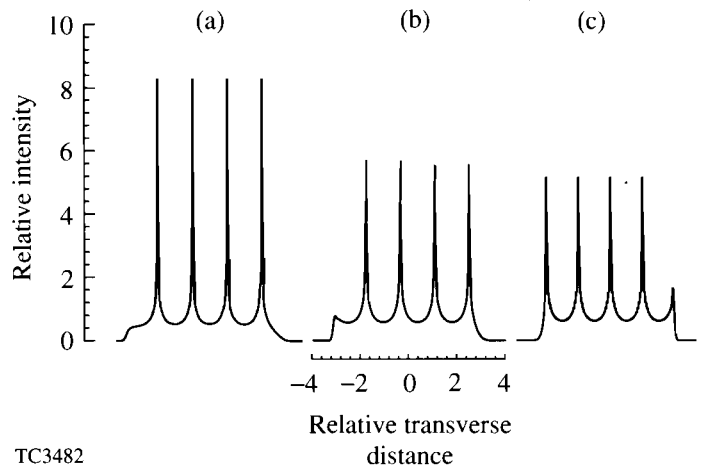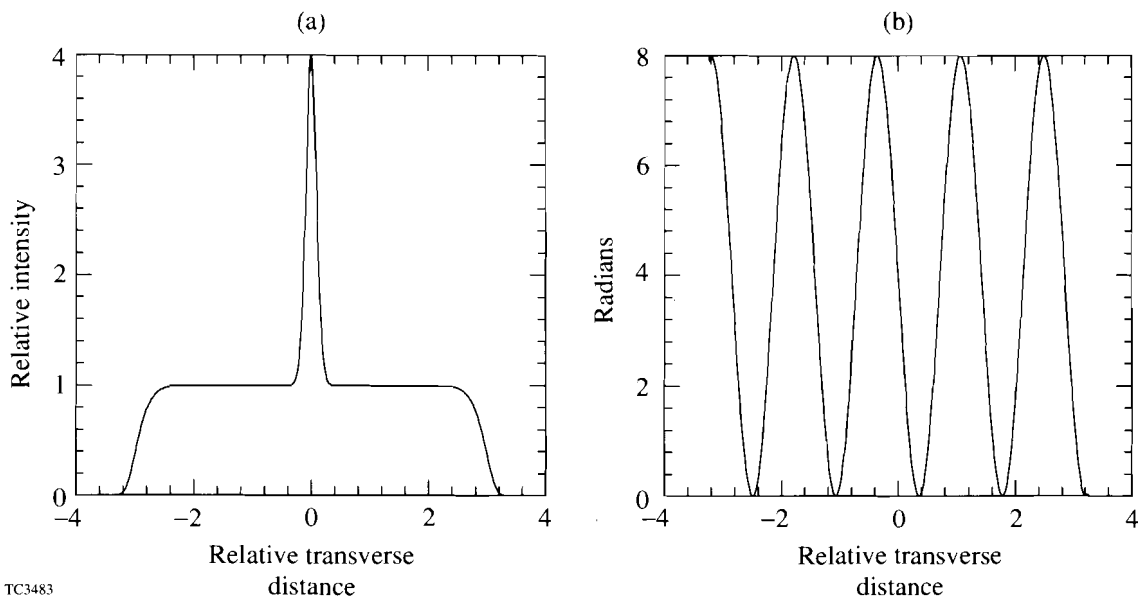
Fig. 56.8

Comparison of self-focused intensity profiles due to monochromatic and converging and diverging SSD beams in a nonlinear medium. (a) Intensity profile due to a diverging SSD beam; (b) intensity profile due to a monochromatic beam; (c) intensity profile due to a converging SSD beam.

These results represent instantaneous modulation development along a wave front propagating through the system. However, it is important to remember that the phase modulation, and hence the resultant amplitude modulation, is time dependent. The transverse position of an amplitude spike will be shifted on succeeding wave fronts. As such, the spikes will smooth out when the intensity is averaged over one E-O modulation period. An example of this smoothing will be shown in the next subsection.

2. Intrinsic Sources of Amplitude Modulation

The last situation to examine is when an SSD beam samples a defect in the laser system that serves as a source of additional intensity perturbations. Of interest is whether the presence of SSD serves to enhance or reduce the amount of self-focusing that these perturbations would suffer upon injection into a nonlinear material. To examine this problem, we first initialize an SSD beam with a well-defined amplitude spike [as shown in Fig. 56.9(a)] and then propagate it in air. (Here we have assumed that the defect produces the same percentage amplitude modulation for each spectral component.) Of particular importance is the spatial alignment of the amplitude spike with the phase distribution of the SSD beam given in Fig. 56.9(b). Depending on the phase distribution at the amplitude spike, energy can be directed into or out of the spike, and the whole spike can be deflected as the wave propagates. (This is due again to optical ray propagation perpendicular to the wave front.) The defect will be deflected from side to side as the gradient in phase across it alternates its direction in time. This gives the impression of the intensity spike sweeping spatially in time with a period equivalent to that of the E-O modulation frequency. This excursion about the original axial location of the defect results in the time-averaged intensity being lower than the initial defect intensity. Figure 56.10 illustrates this effect.

The profile shown in Fig. 56.9(a) was propagated 300 cm and resulted in the profile given in Fig. 56.10(a). It can be seen that the background intensity has suffered the usual modulation due to SSD propagation. At this particular time,

TC3483

Fig. 56.9
Spatial intensity profile used to examine the effects of SSD on the self-focusing of intrinsic amplitude modulation within a laser system. (a) Initial intensity profile with a 4-to-1 spike modulation; (b) spatial profile of the SSD relative phase distribution sampling the intrinsic spike modulation.
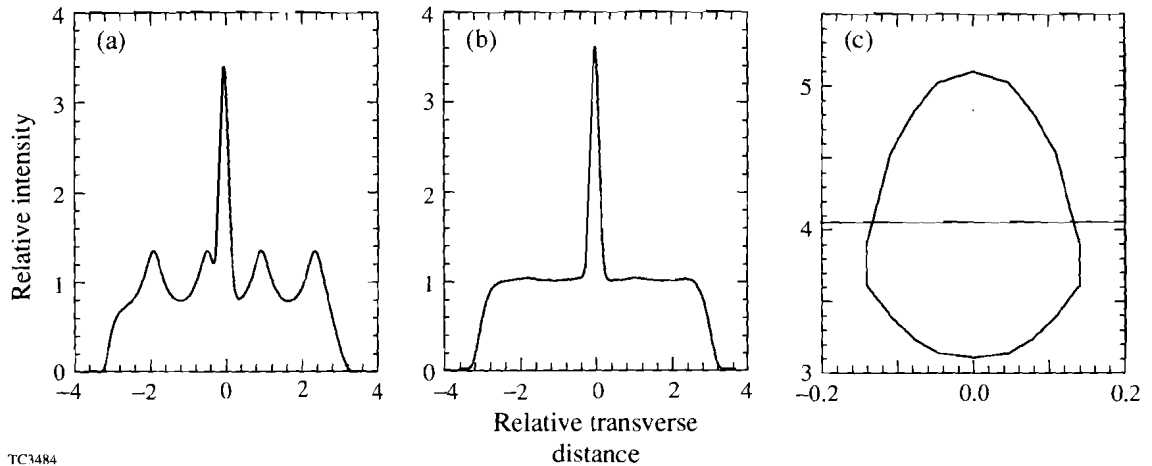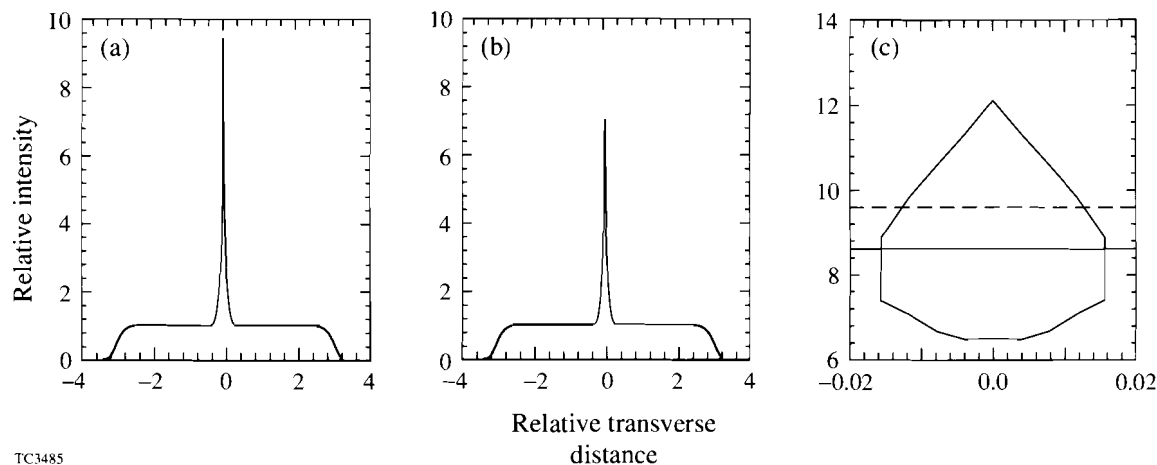
Fig. 56.10
Intensity profiles due to SSD propagation in air for 300 cm. (a) Instantaneous intensity profile. Note the modulated background and reduced and spatially shifted peak. (b) Time-averaged intensity profile after one period of the modulation. The background amplitude modulation has been smoothed, and the peak intensity has been reduced from an initial value of 4. (c) Excursion map of the peak intensity as a function of its spatial position over a single period of the modulation frequency. The solid horizontal line represents an effective peak intensity for the excursion period.

the intensity of the initial spike has been reduced, while its position has been shifted left of the original defect location in the center of the beam. A series of runs were compiled for several times during a single period of the E-O modulator frequency to generate the time-averaged intensity shown in Fig. 56.10(b). Two important features can be seen from this graph. First, as was indicated earlier, the instantaneous modulation of the background intensity due to SSD propagation has been smoothed over the E-O period. Second, the time-averaged intensity of the spike has been reduced to a level lower than its original value. This second point can be explained by examining an excursion map of the spike intensity as a function of its deflected spatial position [Fig. 56.10(c)]. We take the average intensity contribution of the spike at each position in Fig. 56.10(c) to determine an effective spike intensity during the period. This effective intensity is represented by the horizontal line drawn across the graph in Fig. 56.10(c). (The actual dependence is parabolic, is centered at the origin, and has a 10% peak-to-valley variation.) In this case it can be seen that the effective intensity is equal to the initial defect intensity. The lower average intensity is then due to this effective intensity sweeping back and forth across the excursion region during a simple period. Although the time-averaged intensity is lower than the original defect intensity, the excursion map shows that the magnitude of the instantaneous intensity can, at times, be greater than that of the original perturbation. This is the case when the position of the initial defect spike becomes subject to growth due to the SSD propagation modulation.

Knowing the behavior of the beam in air, we can now examine the problem of the beam propagating in a nonlinear material. The profile given in Fig. 56.9(a) was propagated 70 cm in a nonlinear medium $\left(\gamma = 2.9 \times 10^{-7} \text{cm}^2/\text{GW}\right)$ with the results shown in Fig. 56.11. Figure 56.11(a) shows a reference monochromatic beam in which the defect spike has experienced more than a factor-of-2 increase in intensity. A series of runs were again compiled for the SSD beam for many times during a single period of the modulator. The averaged results, shown in Fig. 56.11(b), indicate that the self-focused SSD beam has an average intensity that is lower than the reference monochromatic case. Examining the excursion

Fig. 56.11
Intensity profiles due to SSD propagating
70 cm in a nonlinear material
$\left(\gamma = 2.9 \times 10^{-7} cm^2/GW\right)$. (a) The self-focused intensity profile due to the propagation of a monochromatic beam. The initial peak intensity of 4 has more than doubled at this point. (b) Time-averaged, self-focused intensity profile due to an SSD beam. While the SSD beam has experienced self-focusing, its magnitude is less than the monochromatic case above. (c) Excursion map of the peak self-focused intensity over a single period of the modulation frequency. The dotted line indicates the value of the peak self-focused intensity given in (a). The solid line represents an effective peak intensity for the excursion period.

map [Fig. 56.11(c)], we have added a dotted horizontal line that indicates the value of the self-focused monochromatic beam. It should be noticed that the effective spike intensity (solid line) is lower than this value. This difference is due to the nonlinear response of the medium. When the spike intensity is reduced due to SSD laterally shifting its energy away, it has far less opportunity to self-focus than in the case of when SSD shifts energy into the spike. While the latter case yields an instantaneous self-focused intensity that is greater then the monochromatic case, the combination of the two, because the lower value has not kept pace, gives an effective intensity that is lower than the monochromatic case. As before, the average intensity is lower than the effective intensity due to the effective intensity sweeping over the excursion region. Finally, we have propagated a distance for the beam to exhibit a respectable amount of self-focusing but with only a modest amount of instantaneous propagation modulation. However, as in the case for air, one can expect that any amount of this type of modulation will smooth out over the E-O modulation period.

Conclusions

The need for good irradiation uniformity in ICF target implosions has led to the development and application of several beam-smoothing techniques that employ BBW light. In conjunction with BBW light, SSD applies spectral angular dispersion to produce smooth beam envelopes in the target plane. While SSD produces very smooth beams over times comparable to the E-O modulation frequency, the beams may develop instantaneous amplitude modulation as they propagate through the laser system. The understanding of how such beams behave as they propagate within the nonlinear media of the laser can be important to prevent damage in glass components.

We have developed a multidimensional, multifrequency computer code to examine the propagation of a BBW beam with applied angular dispersion through a laser system. Results from this computer simulation indicate that, for a given set of SSD parameters and nonlinear material, the SSD beam must be propagated a minimum threshold distance before self-focusing (defined as a gain

coefficient of 0.5% cm^{-1}) of its modulation will occur. For distances greater than this minimum, SSD will further contribute to self-focusing when the beam is diverging during image relaying and will reduce the self-focusing when the beam is converging. However, in both cases, the time-averaged intensity is very smooth when averaged over one E-O modulation period.

Simulation results indicate that for imposed amplitude perturbations due to laser imperfections, the SSD beam will, at times, yield a peak instantaneous perturbed intensity that exceeds either the initial perturbed intensity in the case of propagating in a linear material or the self-focused intensity of a similarly perturbed monochromatic beam in the case of propagating in a nonlinear material. In both cases, however, results confirm the time-averaged perturbed intensity is reduced during propagation by the presence of SSD on the beam.

ACKNOWLEDGMENT

REFERENCES

1. Y. Kato *et al.*, Phys. Rev. Lett. **53**, 1057 (1984).

2. T. Kessler *et al.*, LLE Rev. **33**, 1 (1987).

3. R. H. Lehmberg, A. J. Schmitt, and S. E. Bodner, J. Appl. Phys. **62**, 2680 (1987).

4. R. S. Craxton, S. Skupsky, and J. M. Soures, LLE Review **36**, 158 (1988).

5. S. Skupsky, R. W. Short, T. Kessler, R. S. Craxton, S. Letzring, and J. M. Soures, J. Appl. Phys. **66**, 3456 (1989).

6. R. W. Short and S. Skupsky, IEEE J. Quantum Electron. **26**, 580 (1990).

7. R. W. Short (private communication).

8. T. Kessler (private communication).

9. A. Yariv, *Quantum Electronics*, 2nd ed. (Wiley, New York, 1975), Sec. 14.4.

10. L. A. Vainshtein, Sov. Phys.-Tech. Phys. **9**, 157 (1964).

11. Y. R. Shen, *The Principals of Nonlinear Optics* (Wiley, New York, 1984), p. 242.

12. W. W. Simmons, J. T. Hunt, and W. E. Warren, IEEE J. Quantum Electron. **QE-17**, 1727 (1981).

13. V. I. Bespalov and V. I. Talanov, JETP Lett. **3**, 307 (1964).

14. J. R. Jokipii and J. Marburger, Appl. Phys. Lett. **23**, 696 (1973).

15. A. Campillo, S. L. Shapiro, and B. R. Suydam, Appl. Phys. Lett. **24**, 178 (1974).

16. E. S. Bliss *et al.*, Appl. Phys. Lett. **25**, 448 (1974).

17. S. A. Akhmanov, R. V. Khokhlov, and A. P. Sukhorukov, in *Laser Handbook*, edited by F. T. Arecchi and E. O. Schulz-Du Boi (North Holland, Amsterdam, 1972), p. 1168.

18. H. F. Talbot, Lond. and Edin. Phil. Mag. and J. of Sci., Vol. 9, **56**, 401 (1836).